ADVANCED CFD ANALYSIS OF 14-BIS AIRCRAFT

Leonardo Ostan Bitencourt
Instituto Tecnológico de Aeronáutica, CTA/ITA/IEA, São José dos Campos
lostan@gmail.com

Ramon Morais de Freitas
Instituto Nacional de Pesquisas Espaciais, INPE, São José dos Campos
ramon@dsr.inpe.br

Grégori Pogorzelski
Instituto Tecnológico de Aeronáutica, CTA/ITA/IEA, São José dos Campos
gpogor@gmail.com

João Luiz F. Azevedo
Instituto de Aeronáutica e Espaço, CTA/IAE/ASE-N, São José dos Campos
azevedo@iae.cta.br

Abstract. *The present work describes the preliminary results of a CFD-based first analysis of the 14-Bis aircraft aerodynamics. The discretised fluid domain was built around a simplified geometric CAD model of this airplane and the proper boundary conditions were prescribed according to reported historical flight conditions. An implicit, Navier-Stokes solution algorithm, for which both time-marching scheme and spatial discretisation are 2nd order accurate, was used to solve the turbulent flow on unstructured grids. The test cases are concerned with lift and drag prediction, parametric flight speed and longitudinal stability analysis. The preliminary results lead to qualitative agreement with historical reports, although a different computational flight speed has been determined.*

Keywords: *Aerodynamics, CFD, Centennial of Flight, Santos Dumont, 14-Bis*

1. Introduction

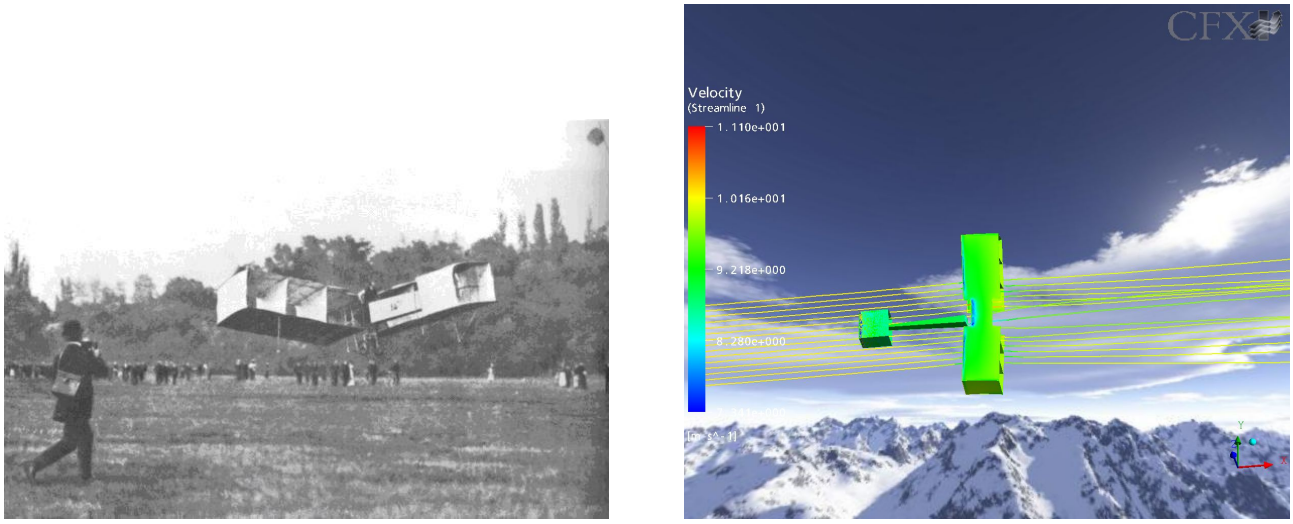

(a) 14-Bis in flight 23 October 1906 - Source: Museu Aeroespacial.

(b) CFD simulated model over the mountains.

Figure 1. The historical first flight and a CFD simulated model.

On October 1906, in the Bagatelli Field, Paris, France, Santos Dumont flew the 14-Bis aircraft and won the Deutsch-Archdeacon Prize. The 14-Bis aircraft was constructed from pine and bamboo poles covered with Japanese silk. The

aircraft had a complex canard-biplane configuration, which was a construction based on Hargrave‘s box kites. The Hargrave cell in the nose pivoted up and down to act as an elevator and from side to side in the role of a rudder. The wings were rigged with 10 deg. of dihedral and the first flights were made without ailerons. The preliminary flight test happened with the 14-Bis aircraft attached to the No 14 dirigible, while explains its designation.

The 14-Bis flew without the dirigible on September 13, 1906, making a hop of between 6 and 13 meters. On October 23, Santos Dumont managed to fly for 60 meters, and this is the flight illustrated in the left of Fig. 1. Then, on November 12, he flew 220 meters in 21-1/2 seconds with members of the Aero-Club de France in attendance. Santos Dumont won a prize of 1500 francs for making the first flight in Europe over 100 meters. Since he was observed by officials from what would become the Federation Aeronautique Internationale, Santos Dumont was credited with making the first heavier-than-air powered flight.

The original power-plant was a 24 hp Antoinette engine, but this was upgraded to the 50 hp version from October after take off tests during September (Vilares, 1956). The main 14-Bis geometric characteristics are presented in Tab. 1.

Table 1. Historical 14-Bis Geometric Characteristics.

Total Canard Area	8 m^2	Length	10 m
Canard Chord	2 m	Engine Power	24 hp(first) - 50 hp
Canard Span	2 m	Weight with pilot	$\approx 300kg$
Wing Chord	2.5 m	Historical Cruise Flight Speed	9 to 12 m/s
Wing Span	11.50 m	Wing Chord Reynolds	10^7
Wing Dihedral	10 deg.	Canard Chord Reynolds	10^7
Total Wing Area	50 m^2	Canard-Wing Distance	5 m

During a long time, there were just two approaches to the aerodynamic study, the wind tunnel testing and the analytical solution of the simplified Navier-Stokes equations. The last method is very limited, just some simple cases can be predicted with acceptable accuracy. The wind tunnel also has some disadvantages as higher energy consumption, much time is spent performing the tests, constructing the model and processing the data results. Moreover, only some flow conditions can be reproduced. It must be pointed that those factors together are related to more costs.

The CFD techniques emerge as an alternative able to reduce project costs, since time and money spent with wind tunnel testing are substantially reduced. In addition to this, CFD has the advantage of numerically solve the fluid equations, although into a discretised domain, it’s possible to locally visualize the flow properties in a way much more detailed than any wind tunnel visualization techniques could show. But, in spite of CFD advantages, wind tunnel tests still are an indispensable stage of every aircraft project, since this is as similar to physical reality as possible.

The main objective of this article is to apply computational fluids dynamics techniques for aerodynamic analysis of the 14-Bis aircraft. As a preliminary test, CFD techniques are used for evaluation of the aircraft configuration and, in particular, extract aerodynamics coefficients. Standard CFD simulations using Navier-Stokes equations were applied for several conditions which involve variations of angle of attack, and historical velocities. The results show $C_L \times \alpha$, $C_L \times C_D$, $L \times V$ and $D \times V$ curves.

2. Theoretical Formulation

2.1 Reynolds-Averaged Navier-Stokes Equations

These equations constitute the more general flow formulation for which the fluid continuum hypothesis can be assumed. The Navier-Stokes equations, for a perfect gas, without the generation of heat and with negligible field forces can be written as

$$\frac{\partial \rho}{\partial t} + \frac{\partial (\rho u_j)}{\partial x_j} = 0 \quad , \tag{1}$$

$$\frac{\partial (\rho u_j)}{\partial t} + \frac{\partial (\rho u_j \, u_i)}{\partial x_j} + \frac{\partial p}{\partial x_i} - \frac{\partial \tau_{ij}}{\partial x_j} = 0 \quad , \tag{2}$$

$$\frac{\partial e}{\partial t} + \frac{\partial [(e+p)\, u_j - \tau_{ij}\, u_i + q_j]}{\partial x_j} = 0 \quad , \tag{3}$$

where ρ, p and $\vec{u}$ are the fluid density, pressure and velocity, respectively, $\vec{\vec{\tau}}$ is the viscous stress tensor, $\vec{q}$ is the heat flux vector and t is the time. The term e is the total energy per unit of volume, given by

$$e = \rho \left[e_i + \frac{1}{2}(u^2 + v^2 + w^2) \right] \quad , \tag{4}$$

where u, v and w are the velocity vector Cartesian components and e_i is the internal energy.

In the formulation, two assumptions were adopted: the absence of heat transfer, i.e., the heat flux vector terms equal zero, and the flow was treated as imcompressible due to the low flow Mach numbers values (lower than 0.05). To save computational memory and processing capabilities the turbulent flow analysis is performed using the Reynolds-Averaged Navier-Stokes equations.This is done by rewriting the Navier-Stokes equations into a form called Reynolds Average Navier-Stokes equations. These equations contain the mean variables and a certain number of terms representing the turbulence effects that must be modeled.

3. Numerical Approach

3.1 Flow Solver

The computations on unstructured grids have been carried out by CFX (see CFX, 2005) which is a software capable of performing the analysis and solution of complex internal and external three dimensional flows. The solutions of the turbulent flow regions were based on the Reynolds-Averaged Navier Stokes equations (RANS), supported by the k-ϵ turbulence model (Jones and Launder, 1972).

The CFX solver simulated a steady, viscous and incompressible flow around the 14-Bis model. This code uses a cell-vertex, finite element-based control volume method. An iterative, second order, time marching scheme was used to numerically solve the RANS equations. To decrease the computational time, some convergence acceleration techniques, such an algebraic multigrid (MG) procedure and parallel computations, were used during the simulations.

3.2 Grid Generation

The 14-Bis CAD geometry was generated from planform and historical source observations. The authors have tried to express the real forms of the airplane as much as possible. Around the geometry, the flow domain was discretised using unstructured grids. Since memory and processing capabilities were limited, the geometry was simplified keeping only the main components, i.e.wings, canard and fuselage. Figure 2 makes a parallel between the original geometry and the simulated one.

The grid generator software used, ICEM-CFD (2005), allows the automatic generation of the hexahedral grid, but the superficial mesh over the airplane had a poor arrangement. Then, the strategy adopted was first create a structured 2-D grid over the geometric surface. After that, the Delauney method (Field,1987) was applied, generating the desired unstructured volumetric grid. To assure a faster convergence and a good solution, the mesh quality must be taken into account. Therefore, the element transitions were performed gradually. Furthermore, regions of leading edges, trailing edges and the ones containing wakes received grid refinement to avoid spurious solutions.

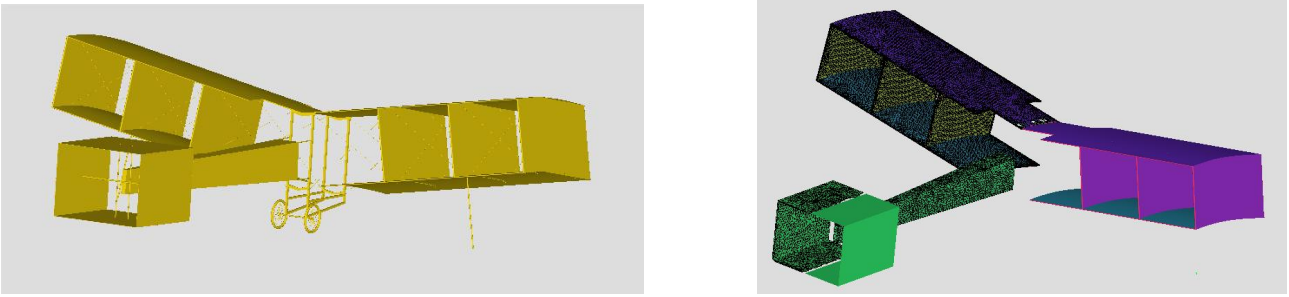

(a) Original CAD model. (b) Mesh view of idealized configuration.

Figure 2. Comparative view of the original CAD model and simulated configuration

3.3 Boundary Conditions

The correct application of boundary conditions is vital to properly close the boundary problem, assuring correct problem modeling. For the 14-Bis aircraft simulation basically four different boundary conditions were used: INLET, OUTLET, OPENING and NO-SLIP WALL. The nomenclature use here is adopted by the CFX solver.

INLET condition was applied on the computational domain entrance surface. Over there, the freestream velocity and the direction are specified. NO-SLIP WALL condition assured that neither tangential or normal velocity were present on aircraft surface. The OUTLET condition was used to model the fluid flow exit at the domain. The OPENING boundary condition modeled both entrance and exit fluid flow. The form in which all of these conditions were prescribed to close the problem is listed in Tab. 2.

Table 2. Detailed description of prescribed boundary condition on domain surfaces.

Surface	Type	Description
Aircraft	NO-SLIP WALL	On aircraft surface, the normal and tangential velocity are kept zero.
Entrance	INLET	With the velocity specification it was possible to model freestream conditions.
Exit	OUTLET	The atmospheric pressure was specified as exit pressure.
Lateral sides	OPENING	The atmospheric pressure was also specified.

3.4 Post-Processor for Aerodynamics Forces

The post-processor, by means of simple and useful tools, allows evaluation of aerodynamics forces and the observation of the flow field variables, for example, pressure and temperature fields, streamlines or boundary layer velocity profiles. The resultant force in the airplane, when projected into the wind axis results in drag, lift and yaw forces. The evaluation of these aerodynamic forces is performed by integrating the surface pressure forces and shear stresses as shown in Eq. 5. More detailed description of these method can be found in Cummings et al., 1996.

$$\vec{F}_{near} = \int_{S_{near}} \left[(p - p_\infty)\,\vec{\vec{I}} - \vec{\vec{\tau}} \right] .\vec{n} dS \quad . \tag{5}$$

The aerodynamic drag is a force exerted by the flowfield on the body surface in a direction contrary to its movement. The drag is the summation of the tangential, or skin friction forces, and surface pressures or normal forces, projected into the freestream direction. The drag breakdown with the near-field drag computation approach, as discribed in (Cummings et al., 1996), comprises: pressure and friction drag. The pressure drag can be broken into induced, wave and form drag components, but it is not possible to recover each pressure drag component using only the near-field approach. The relative contribution of each drag component depends on the flight conditions. For example, in the case of attached subsonic flow and zero lift, the friction drag is dominant. The form drag is the result of viscous effects inducing changes in the pressure distribution over the aircraft. It is the dominant component in the case of vehicles with regions of separated flow. The sum of friction drag and form drag is called viscous drag or profile drag.

4. Test Cases

The chosen test cases explore the main aerodynamics characteristics of the 14-Bis airplane. Basically, this parametric study is shown in Tab. 3. Through the angle of attack variation studies it was possible to plot the lift coefficient, drag coefficient and polar drag curves. The canard incidence angle variation can show the downwash effect in the wings. Moreover, stability and controllability of the airplane can be checked. The velocity variation in the entrance of the computational domain was used to find the most probable flight speed, whose value is not exactly known because historical sources are not in agreement. Moreover, these historical registries only take into account the airplane velocity relative to the ground, but it would be more interesting, in an aerodynamic point of view, to obtain the wind relative velocity. Hence, a range of velocities were tested. The interference between the main airplane parts was also checked.

Table 3. Simulated test cases for the parametric study of the main aerodynamic characteristics of the 14-Bis airplane.

Parameter	Variation	Fixed Conditions
V_∞	8 m/s to 12 m/s	Variation of V_∞,α = 0 deg.
α	-7 deg. to +7 deg.	Variation of angle of attack with $V_\infty = 10.21 m/s$

5. Results and Discussion

From the simulation results, it was possible to obtain the aerodynamic drag and lift forces acting over each component (wing, canard and fuselage) and the total forces. Based on the different conditions, curves as $C_L \times \alpha$ for canard and aircraft, besides $C_L \times C_D$ were extracted, allowing the airplane flight analysis in a preliminary way. Figure 3(a) shows the curve $C_L \times \alpha$ obtained from simulations performed for angles of attack between -7 deg. and 8 deg.

The Figure 3(b) shows the curve CL x ALFA obtained for Canard. In the region represented, the curve has a linear behavior.On the other hand, for angles of attack higher than 8 deg, in the region represented, the curve has a linear behavior. On the other hand, for angles of attack higher than 8 deg., unsteady solutions were obtained. This shows that, probably, when the angles of attack are higher than 8 deg., the flowfield must has some quite extensive separation regions.

An aspect that should be pointed out is that the wing incidence angle of approximately 5 deg. was used in the 14-Bis aircraft. From the $C_L \times \alpha$ curve, one can see that to at a 0 deg. angle of attack corresponds C_L = 0.9. As the maximum 14-Bis wing profile camber is only 5%, the C_L value obtained is justified by the wing incidence angle. Moreover, from the same curve, the value $C_{L\alpha} = 4.83$ was obtained.

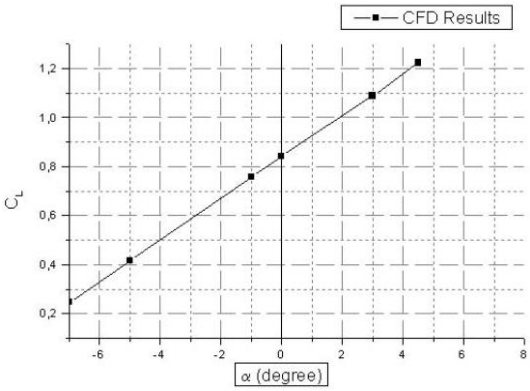

(a) Aircraft $C_L \times \alpha$ curve. Reference area $S_{ref} = 28.75\,\mathrm{m}^2$.

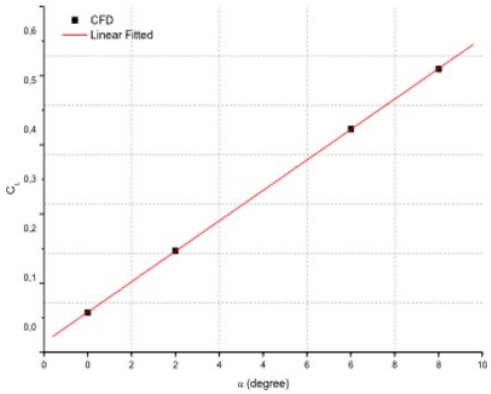

(b) Canard $C_L \times \alpha$ curve.

Figure 3. The $C_L \times \alpha$ curves for canard and entire aircraft used to further analysis.

The airplane drag polar shown on Fig. 4 (b) received a parabolic curve fit. An important observation, that must be addressed with respect to the drag polar and the general drag results obtained is concerned with the geometric simplifications assumed in the simulated model. One can expect that the missing structure components, such as struts, landing gear and even the pilot, should increase the drag when compared to the numerical calculations. Nevertheless, the computational drag polar still gives enough information to a first analysis of the airplane, allowing reasonable drag predictions when simulating the historical flight conditions.

It was estimated by Vilares (1956) that the 14-Bis aircraft first flight speed was about 11 m/s. It must be pointed out that this is a mean speed value using the ground as reference.The wind influence over the airplane speed was not considered. Therefore, the aerodynamic speed could be different from the historical measured value of 11 m/s. In addition to that, there is also the speed variation during the acceleration procedure. From all of this information, it is possible to conclude that the true air speed could in reality have been higher than the estimated mean value. With the objective of having a better estimative of the most probable speed values, a parametric analysis of this variable influence over the aircraft lift and drag was performed.

Figure 4(a) contains the lift curves as a function of the aerodynamic speed at different angles of attack. According to Greco and Ribeiro (2003), the aircraft weight was about $300kg$. Therefore a lift force higher than $3000N$ should have been generated to allow the flight. The horizontal line plotted in Fig. 4 (a) represents the minimum lift that must be produced at a specific speed and angle of attack in order to allow sustained flight. From this figure it is possible to verify that the minimum lift is reached by speeds of 14.5 m/s and 11.5 m/s with 0 deg. and 5 deg. of angle of attack, respectively.

Another important parameter to analyze the flight envelope is related to the observation of drag force variation as a function of aerodynamic speed. Figures 5(a) and 5(b) show the drag values obtained by speeds between 0 m/s and 16 m/s at different angles of attack. The required force to balance the drag force during flight must be generated by the aircraft engine using the propeller capability to transform the shaft power into traction. Historical sources pointed by Vilares (1956), indicate that Santos Dumont first used a 24 hp nominal power engine. The power deficiency of this engine became evident in September 1906 during a flying attempt, when the aircraft, in spite of some jumps, was unable to take off. During the following experiments, a new and more powerful engine was selected. Its nominal power was 50 hp at 1500 rpm (Vilares, 1956).

Other important point about the 14-Bis performance is the propulsive efficiency (η_p), whose value is unknown. It is important to note that the thrust produced by the engine vary with flight speed, decreasing with the speed increment. As the blades do not convert completely the given engine shaft power, three isolines of different η_p, whose values are $20\,\%$, $30\,\%$ and $50\,\%$, were plotted. These values are in agreement with the historical records (Vilares, 1956). In Fig. 5(b), the black lines are the efficiency isolines, for the engine power fixed at 50 hp. The color lines, one for each angle of attack, give the drag for each flight speed. The curves indicate, for the smallest propulsive efficiency ($\eta_p = 20\,\%$), that the airplane has enough thrust to reach flight speeds up to 12 m/s at $\alpha = 5$ deg., where there is enough lift for sustained flight, as previously discussed. For a propulsive efficiency of $\eta_p = 30\%$, the airplane could reach speeds of 14 m/s at

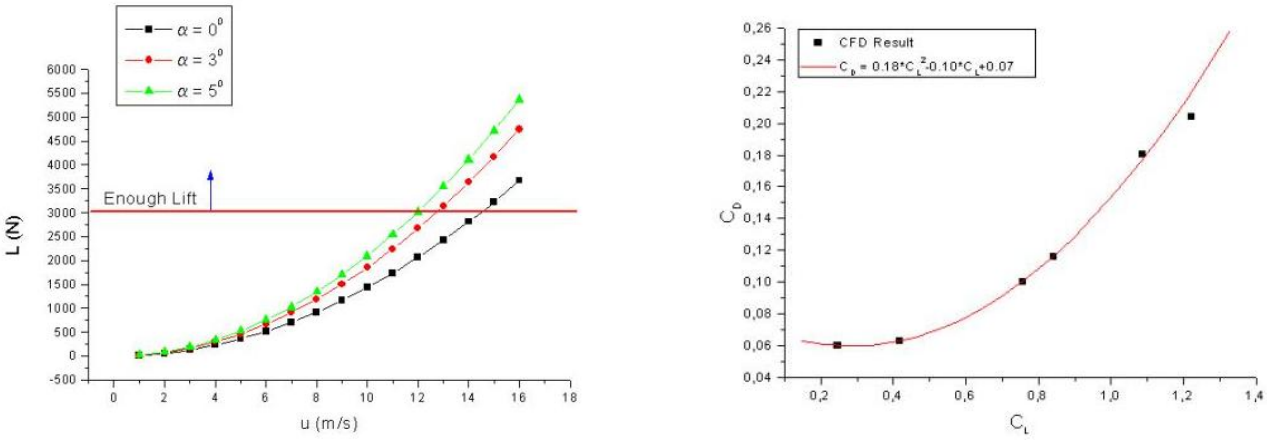

(a) Lift dependence with flight velocity.

(b) Drag polar.

Figure 4. Lift dependence with flight velocity and drag polar curve.

$\alpha = 5$ deg., or even higher speeds at lower values of α.

Some factors should be carefully observed about drag and thrust estimated values. The first point to be considered is that due to geometric simplifications, the CFD drag results were probably lower than the actual drag in flight. Therefore, the colored curves in Figs. 5(a) and 5(b) should be shifted upward, restricting the admissible flight speed range and bringing the probable flight speed closer to the reported historical flight speed. Despite that fact, during take-off, the ground causes additional drag forces but there are also lift increments due to ground effect. Neither of those effects were considered in the analysis.

In spite of the produced thrust, it is possible that the true engine power does not match with the indicated value, i.e., 24 hp or 50 hp. This fact also decreases the admissible flight speed for the expected angles of attack. Therefore, according to the historical reports of flight speed, the available thrust should not be the critical factor to allow the flight. In Fig. 5(a), a plot similar to the one at Fig. 5(b), is shown, but now using propulsive efficiency isolines for the 24 hp power engine, which was used in the first 14-Bis take-off attempt. Through the observation of Fig. 5(a), it is possible to conclude that the maximum achievable speed is 13 m/s when at 5 deg. of angle of attack and using a propeller with efficiency $50\,\%$, corresponding to a 3700N lift force as seen in Fig. 4(a). In the case of a lower efficiency, for example 30%, the maximum speed would be 11.3 m/s, generating a lift of only 2700 N, insufficient to counteract the aircraft weight. This explains the flight failure when the less powerful engine was used. The example stated also represents that, when the flight velocities are being analyzed, both the thrust requirements, Fig. 5(b), and the lift requirements, Fig. 4(a), must be taken into account.

6. Preliminary Longitudinal Static Stability Analysis

Stability is possibly the most critical part of the project. The 14-Bis aircraft had a complex canard-biplane configuration. The canard function is to generate enough lift to compensate the moment caused by the wing CG arm. The canard surface was placed well ahead of the center of gravity, creating an extensive de-stabilizing influence. Consequently it was vital that the aircraft CG position has been situated ahead of aircraft neutral point (NP) for longitudinal static stability. For the initial analysis, the position of the aircraft neutral point was estimated. Schlichting and Truckenbrodt (1979), proposes a formula that considers wing and canard surface area, $1/4$ of chord point distance between canard and wing and $C_{L\alpha}$ values relative to canard and aircraft. The result of the canard $C_{L\alpha}$ curve is presented in Fig. 3(b) for the linear regime. Given the relative CG position indetermination, a parametric analysis was performed by varying its position from historical data and getting the values of $C_{M\alpha}$ and static margin, as demonstrated in Table 4. The aerodynamics linear regime for canard and wing is considered. The estimated neutral point position seems to be coherent with the historical reports, demonstrating that a small CG position variation modifies the aircraft longitudinal stability. This could have been the 14-Bis aircraft crash cause during its last flight on April 1907.

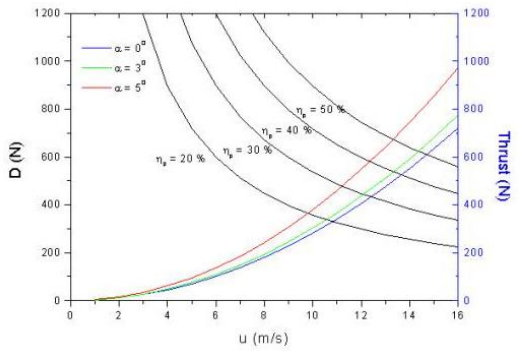

(a) Drag dependence with velocity and 24 hp engine thrust curves.

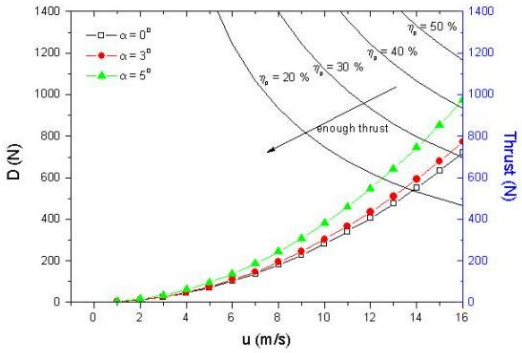

(b) Drag dependence with velocity and 50 hp engine thrust curves.

Figure 5. Curves used to study the influence of engine power into flight performance.

Table 4. Parametric longitudinal static stability analysis

Center of Gravity Position[(1)]	Cm_α[(2)]	Static Margin (%)	Stable
6.5	-2.64	44.89	Yes
6.6	-2.16	40.00	Yes
6.7	-1.68	34.14	Yes
6.8	-1.20	27.02	Yes
6.9	-0.72	18.18	Yes
7.0	-0.24	6.89	Yes
7.1	0.24	-8.00	No
7.2	0.72	-28.57	No
7.3	1.20	-58.82	No
7.4	1.68	-107.69	No
7.5	2.16	-200.00	No

(1): Reference point is aircraft nose.
(2): Neutral Point Position = 7.05 meters.

7. Conclusion

This work has shown preliminary analysis, using CFD techniques, for evaluation of the 14-Bis aircraft configuration. The historical flight conditions were simulated using the finite volume method and solving the RANS equations with the k-ϵ turbulence model. A geometric simplified model of the aircraft was used and the results obtained so far seem to be in pretty good agreement with the historical reports.

The discussion presented in the previous section confirmed why the 24 hp power engine was unable to make the 14-Bis take off during the first flight attempt in September 1906. Therefore, the engine change, selecting a more powerful one (50 hp), is clearly justified. Based on the present calculations, it is difficult to believe that 11 m/s was the true airspeed of the aircraft, because the lift vs. speed curve, that was generated during the simulations, indicates very restrictive conditions concerning such flight speed. An acceptable speed, assuming a 5 deg. angle of attack, seems to be between 12 m/s and 14 m/s. These speeds could be reached more easily when flying against the wind direction. In any event, it can be stated, based upon the present numerical results, that the flight speeds should have been higher than 12 m/s.

This analysis of longitudinal static stability cosidered the linear regime and shown that the position of the neutral point estimated is coherent with the reality of historical reports. Moreover, the parametric test demonstrated that small center of gravity position variations around the historical point could make the aircraft to become statically unstable. This inicial study about longitudinal static stability does not allow further analysis concerning this topic, although it must be pointed out that the CG position seems to be a critical factor that deserves further analysis. The next step will be to use the CFD tools for studies of the nonlinear region of the $C_{L\alpha}$ curve, for example, the canard response in high angle of attack.

8. Acknowledgments

The authors are indebted to Prof. Paulo Greco, from Escola de Engenharia de São Carlos, Universidade de São Paulo, who provided the geometrical CAD model, and to Mr. Marcus Reis, from Engineering Simulation and Scientific Software, ESSS, who provided support and licences for all used software. The authors acknowledge the partial support of Conselho Nacional de Desenvolvimento Científico e Tecnológico, CNPq, through the Integrated Project Research Grant No. 501200/2003-7. The support of Fundação de Amparo à Pesquisa do Estado de São Paulo, FAPESP, through the Research Grant No. 2000/13768-4, is also gratefully acknowledged.

9. References

CFX, 2005 "CFX SITE", www-waterloo.ansys.com/cfx/.

Cummings, R.M, Giles, M.B. and Shrinivas, G.N., 1996, "Determination of Drag from Three-Dimensional Viscous and Inviscid Flowfield Computations", AIAA-96-2482.

Field, D.A.,1987, "Laplacian Smoothing and Delaunay Triangulations.", Communications of Applied Numerical Methods, Vol.4, pp. 709-712.

Greco, P.S. and Ribeiro, M.L., 2003, "Estudo das Características Aerodinâmicas, de Estabilidade e de Controle do 14-Bis", EESC-USP, Relatório Técnico FAPESP n^o 01/111158-7.

ICEMCFD, 2005 "ICEMCFD SITE", http://www.icemcfd.com/icemcfd.html.

Jones, W. P. and Launder, B. E., 1972, "The Prediction of Laminarization with a Two-Equation Model of Turbulence", International Journal of Heat and Mass Transfer, Vol.5, pp. 301-314.

Schlichting, H. and Truckenbrodt, E., 1979, "Aerodynamics of the Airplane", McGraw-Hill, New York.

Vilares, H. D., 1956, "Quem Deu Asas ao Homem", Instituto Nacional do Livro, Rio de Janeiro.

10. Responsibility notice

The authors are the only responsible for the printed material included in this paper